

# Modeling Near-Road Air Quality Using a Computational Fluid Dynamics Model, CFD-VIT-RIT

Y. JASON WANG AND K. MAX ZHANG\*

Sibley School of Mechanical and Aerospace Engineering,  
Cornell University, Ithaca, New York 14853

Received May 27, 2009. Revised manuscript received August 19, 2009. Accepted August 22, 2009.

It is well recognized that dilution is an important mechanism governing the near-road air pollutant concentrations. In this paper, we aim to advance our understanding of turbulent mixing mechanisms on and near roadways using computation fluid dynamics. Turbulent mixing mechanisms can be classified into three categories according to their origins: vehicle-induced turbulence (VIT), road-induced turbulence (RIT), and atmospheric boundary layer turbulence. RIT includes the turbulence generated by road embankment, road surface thermal effects, and roadside structures. Both VIT and RIT are affected by the roadway designs. We incorporate the detailed treatment of VIT and RIT into the CFD (namely CFD-VIT-RIT) and apply the model in simulating the spatial gradients of carbon monoxide near two major highways with different traffic mix and roadway configurations. The modeling results are compared to the field measurements and those from CALINE4 and CFD without considering VIT and RIT. We demonstrate that the incorporation of VIT and RIT considerably improves the modeling predictions, especially on vertical gradients and seasonal variations of carbon monoxide. Our study implies that roadway design can significantly influence the near-road air pollution. Thus we recommend that mitigating near-road air pollution through roadway designs be considered in the air quality and transportation management. In addition, thanks to the rigorous representation of turbulent mixing mechanisms, CFD-VIT-RIT can become valuable tools in the roadway designs process.

## Introduction

Elevated air pollutants concentrations have been measured in congested urban areas and near roadways (1, 2), which have been associated with adverse human health effects (3). These effects vary with levels of human exposure to traffic-related air pollutants through different activities (e.g., driving on the road, living/working near or away from the road) (4, 5). Therefore, it is important to understand the spatial gradient of pollutants near roadways, which requires measurements and simulations addressing complex road configurations and meteorological conditions (6, 7).

Dilution is the dominant mechanism for changing the near-road concentrations. Pollutant dispersion near roadways usually experiences two distinct stages -- 'tailpipe-to-road' and 'road-to-ambient' (8). The dilution ratio of the

first stage usually reaches up to about 1000:1 in around 1–3 s; for the second stage, the dilution ratio is usually about 10:1, and the process usually lasts around 3–10 min (8). The aerosol processes such as nucleation, condensation, and coagulation are strongly coupled with dilution (8). For nitrogen oxides (NO<sub>x</sub>), the concentrations change results from the coupling of dilution and chemical reactions (9). For carbon monoxide (CO), an inert species under typical atmospheric conditions, dilution is the only governing mechanism. Therefore CO is usually used as a dilution indicator since it comes mostly from vehicle exhaust and can be easily measured (10).

Dilution is caused by on-road and near-road turbulent mixing. Given the importance of dilution on near-road air quality, it is imperative to gain a better understanding of the mechanisms contributing to the turbulent mixing. Several mechanisms affect the generation of turbulence near roadways besides atmospheric boundary layer turbulence (ABLT) (11). First, the movement of vehicles on the road results in a significant increase in turbulence, which is known as vehicle-induced turbulence (VIT) (11–13). Second, turbulence can be generated by the embankment on which a roadway is located when wind flows over it (15). Third, thermal effects caused by solar radiation generate turbulence during hot season and cannot be ignored for pollutant dispersion (16–18). Fourthly, road structures (i.e., noise barrier, tree planting) can also produce turbulence that influences the flow field (6, 19, 20). Since these three effects can be attributed to roadway design, we refer to them as RIT in this paper.

Gaussian plume-based dispersion models such as CALINE4 and AERMOD have been widely used to assess the pollutant concentrations of urban road environments (21–24). These models typically treat the region directly above the roadway and at prescribed distances on each side of the roadway as a zone of uniform emissions and turbulence called a "mixing zone" (21). The introduction of the "mixing zone" concept is equivalent to a fixed VIT, i.e., not adjustable to the specific roadway conditions (e.g., the different vehicles speeds and types). Their dispersion parametrizations are based in part on roadway geometry and wind direction, but they face the challenge of how to incorporate the effect of road configurations exactly (14, 25–27). In recent years, computation fluid dynamics (CFD) has been applied in modeling the dynamical and mechanical processes taking place in complicated urban street canyons and road tunnels (16, 28, 29). However, it has been rarely applied to simulate near-road air quality, and the comprehensive representation of VIT and RIT is scarce (27, 30).

In this paper, we aim to investigate the effects of different turbulent mixing mechanisms on dilution near roadways. An improved CFD with detailed treatment of VIT and RIT, namely CFD-VIT-RIT, is used to simulate the horizontal and vertical dispersions of CO in the vicinity of two highways during two seasons. The modeling results are compared with field measurements, CALINE4, and a CFD model without considering VIT and RIT. The implications of our findings on future road design and the advantages and disadvantages of applying different dispersion models are also discussed.

## Mechanisms for on-Road and near-Road Turbulence Generation

In this section, we provide a brief summary of the mechanisms that generate VIT and RIT in on-road and near-road environments.

\* Corresponding author phone: (607)254-5403; fax: (607)255-1222; e-mail: kz33@cornell.edu. Corresponding author address: 287 Grumman Hall, Sibley School of Mechanical and Aerospace Engineering, Cornell University, Ithaca, NY 14853.

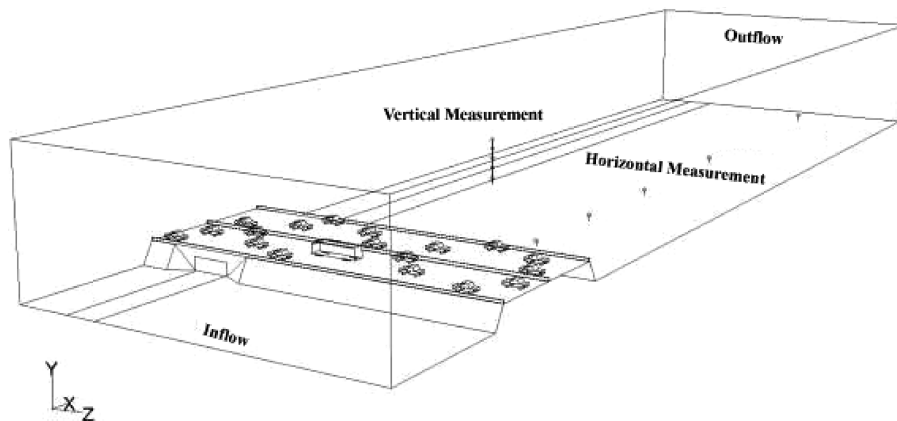


FIGURE 1. Geometric features of the computational domain for I-405.

**Turbulence Induced by Vehicles.** Traffic has a dominant effect in the immediate vicinity of the roadway (14). Moving vehicles enhance mixing processes by inducing turbulence, which originates from the interaction between moving vehicles and ambient air. It is known that up to 50% of kinetic energy is converted into additional turbulence when a fluid hits an obstacle (28). The wakes behind moving vehicles are characterized as momentum wakes and contain organized trailing vortices which play a key role in determining the flux of kinetic energy and rapidly mix the pollutants released in the turbulent wake (14, 31, 32). VIT, which is strongly related to vehicle type and speed (27, 33, 34), can be expected to significantly influence the diffusion of roadway emissions, especially in the microenvironment near roadways (13, 14, 33). VIT increases with vehicle speed, indicating increased wake production of turbulence (14). Experiments also showed that compared with gasoline cars, heavy-duty diesel trucks induce more turbulence due to its size and structure (34).

**Turbulence Induced by an Embankment.** An embankment acts as a topographic obstacle which causes a form drag and produces turbulence to compensate for the deformation of the flow field when wind flows over it (35). A recirculation cavity is created downwind of the embankment, containing a well-mixed, and often lower, zone of pollution concentrations (36). The induced turbulence depends on the wind velocity, wind direction, the height, and the shape of the embankment (15, 33).

**Turbulence Induced by Thermal Effects on Road Surface.** The available solar radiation on a surface,  $Q_0$ , can be divided into turbulent fluxes of sensible heat,  $H_0$ , latent heat,  $V_0$ , and the soil heat flux,  $B_0$  (34). With high absorptivity and low heat capacity, the asphalted surface of roadway receives much net energy. Compared to the grassy or concrete surroundings, it provides a very small latent heat flux and leads to an increased sensible heat flux, which generates turbulence (33). The thermally induced flow is combined with mechanically induced flows and affects the transport of pollutants. It should be noted that due to the large solar zenith angle in the winter, the road surface receives much less direct solar radiation, so the temperature difference between road surface and air can be neglected.

**Turbulence Induced by Roadside Structures.** Roadside structures affect pollutant concentrations around the structure by blocking initial dispersion and increasing turbulence and initial mixing of the emitted pollutants (6, 19, 20). A noise barrier disturbs the wind field as a still obstacle while a tree planting consisting of branches and leaves can be considered as a porous body (6, 19). It has been shown that the plume behind noise barrier and vegetation is relatively uniform and vertically well-mixed, and pollutant concentrations are reduced under certain meteorological conditions. With winds directionally from the road, concentrations of

CO and particle concentrations generally decrease between 15 and 50% behind the noise barrier (6).

### Field Measurements

The experimental data utilized in this paper are collected from previous measurements near Interstate 405 (I-405) and Interstate 710 (I-710) in Los Angeles in the summer and winter (10, 37–40). I-405 is 30 m wide, with an embankment of 4.5 m-height, while I-710 is 26 m wide at ground level. The horizontal sampling points are taken within 300 m downwind and upwind from the center of the highways at height 1.6 m. Meanwhile, the vertical CO concentrations at different heights are measured at 50 m downwind of I-405 in the summer. There are relatively large differences in temperature, but small differences in wind speed and vehicle volume for each highway between different seasons. For I-405, gasoline cars dominate the vehicle mix, while for I-710, more than 25% of the vehicles are heavy-duty diesel trucks. All related conditions are considered in our simulation. More meteorological and road data are listed in the Supporting Information.

### CFD-VIT-RIT

The  $k - \epsilon$  turbulence model available in the CFD code, FLUENT (41), is used for modeling flow and dispersion in the vicinity of roadways and is described in the Supporting Information.

Figure 1 shows the computational domain of I-405 and the sketch of measurement locations. The number of computational cells used for the simulation is 2,305,712, with a size of 380 m by 80 m in the horizontal and 30 m in the vertical direction. The computational domain for I-710 is similar, except that the highway is not located on an embankment. The spatial domain has a size of 380 m by 40 m in the horizontal and 30 m in the vertical direction and is divided into 1,063,541 unstructured cells.

Test zones above road surface are created to obtain average turbulent kinetic energy (TKE). Different heights of the domain are set according to the heavy-duty truck percentage. Since most of the vehicles are cars and vans for I-405, the height of the zone is 2.5 m, while for I-710, the height is 3.5 m since it is a major truck route.

We model the vehicles as real-shaped rather than block-shaped to keep the conditions similar to the streamlined shape of real vehicles (27), since the turbulence for the block-shaped vehicle is estimated to be 25% higher than for the true vehicle models (42). Different types of vehicles are built approximately following their actual sizes. Since the average vehicle speed,  $24 \text{ m s}^{-1}$ , is measured during the experiments (37), the same moving speed for all vehicles is adopted in the simulation (43). For the vehicle surface, an equivalent roughness height of 0.0015 m is chosen to match the

**TABLE 1. Summary of TKE in the Test Zone**

	I-405				I-710			
	summer	percentage	winter	percentage	summer	percentage	winter	percentage
VIT <sup>a</sup>	0.36	41.4%	0.35	53.9%	0.63	76.8%	0.63	95.5%
RIT - embankment <sup>a</sup>	0.30	34.5%	0.27	41.5%	N/A	N/A	N/A	N/A
RIT - thermal effects <sup>a</sup>	0.17	19.5%	N/A	N/A	0.15	18.3%	N/A	N/A
ABLT <sup>a</sup>	0.04	4.6%	0.03	4.6%	0.04	4.9%	0.03	4.5%
total TKE <sup>a</sup>	0.87	100.0%	0.65	100.0%	0.82	100.0%	0.66	100.0%

<sup>a</sup> Unit is m<sup>2</sup> s<sup>-2a</sup>.

simulated drag force of vehicles with the value based on drag coefficient (44). The exhaust pipe is modeled as a small area on the back of the light-duty vehicle or on the top of the heavy-duty diesel vehicles. Since traffic volumes change little between seasons, just one set of vehicles is built for each highway. The embankment for I-405 is built corresponding to its real size (in Figure 1). All the solid boundaries, including ground surfaces and vehicle surfaces, are specified as nonslip boundary conditions in the flow module and are prescribed at a fixed temperature in the heat transfer module. Symmetric boundary conditions (zero gradient normal to boundary) are applied to the top and side faces of the domain. More description of model set up and the figure of meshed vehicles are illustrated in the Supporting Information.

Based on a meteorological study in Los Angeles (45), the temperature difference between air and roadway surface is estimated to be 20 °C for the summer season under strong solar radiation. Considering the atmospheric wind in two seasons, fully developed in-flow vertical profiles for ABLT are incorporated through User-Defined Function (UDF) and described in the Supporting Information.

In summary, we incorporate the turbulence induced by moving traffic, embankment, thermal effects, and atmospheric wind into our model. Since there are no noise barriers and few trees in the surrounding of I-405 and I-710, turbulence generated by the road barriers and trees is not simulated here and will be investigated in future studies.

**Results**

**TKE Results.** Induced TKE within the test zone is summarized in Table 1. From Table 1, it is clear that total TKE changes with seasons and highways and the largest TKE is obtained from I-405 with the embankment in the summer. The produced VIT, especially for I-710, is dominated over ABLT, as suggested by previous wind tunnel studies (46). Due to the large percentage of heavy-duty trucks, VIT of I-710 is much larger than that of I-405. Excellent agreements are found for VIT between our model (0.36 m<sup>2</sup> s<sup>-2</sup> for I-405 and 0.63 m<sup>2</sup> s<sup>-2</sup> for I-710) and the empirical formula (0.37 m<sup>2</sup> s<sup>-2</sup> for I-405 and 0.64 m<sup>2</sup> s<sup>-2</sup> for I-710) reported by Baumer et al. (33). TKE produced by embankment, ~0.30 m<sup>2</sup> s<sup>-2</sup>, or 34.5% of the total TKE in the test zone, is also in good agreement with the value, 0.34 m<sup>2</sup> s<sup>-2</sup>, calculated from the empirical formula in Baumer et al. (33). The large contribution of embankment-induced TKE implies that elevated highways enhance turbulent mixing downwind, potentially reducing human exposure to traffic-generated air pollutants. Furthermore, TKE caused by the thermal effects due to road surface properties accounts for about 20% of total TKE in the test zone and therefore cannot be ignored.

It should be noted that the main advantage of our model over the empirical formula is its capability to resolve the effects of VIT and RIT over the near-road region beyond the test zone. Our simulations show that TKE reaches the maximum value on road and decays with the increasing distance from the highway, until at 300 m it is negligibly small. Due to a large turbulence dissipation rate, VIT,

averaged from the ground to the height of the test zone, drops to below 50% at about 20 m downwind of highway. When wind velocity increases, VIT dissipates faster but is also transported to a greater horizontal distance. When wind velocity is small, VIT can spread to higher elevation. RIT decreases slower than VIT, due to the big size of the embankment which results in a larger influence range. For I-405, the ratio of VIT to RIT decreases with the increasing distance.

**Spatial Gradients of Carbon Monoxide Concentrations.**

In this section, we compare the simulated CO concentrations in both horizontal and vertical directions against the field measurement data. In addition to the CFD-VIT-RIT model, we also present the results from CALINE4 and a standard CFD model. In the standard CFD model, referred to as “CFD” in the text, the highways are treated as elevated line sources without explicit treatment of VIT and RIT. We use 405S, 405W, 710S, and 710W to refer to the studies of two different highways (i.e., I-405 and I-710) at two seasons with “S” and “W” representing summer and winter, respectively.

While the spatial gradients of near-road concentrations of inert species such as CO are determined by turbulent mixing, the absolute concentrations are determined by both vehicle emission factors and turbulent mixing. Since the emission factors derived by models such as MOBILE6 and EMFAC have known discrepancies in representing real-world emission factors (47, 48), our comparisons focus on the relative concentrations of CO, thus avoiding the additional uncertainties introduced by the emission factor models. The CO concentrations at downwind distances are normalized by their values at the closest distances to the roadways, i.e., 30 m for I-405 and 17 m for I-710, respectively. For instance, the relative CO concentrations at 30 m from I-405 are unity for both measurements and modeling results. However, the concentrations at 60 m, 90 m, 150 m, and 300 m vary depending on measurements and selected models.

**Horizontal Gradients and Seasonal Variations.** Figure 2(a) compares the simulation results obtained from the CFD-VIT-RIT, CALINE4, and CFD models to the measurement data for I-405 in the summer. Relative CO concentration decays exponentially when moving away from the traffic source. The dilution between 30 and 60 m varies with different models: CALINE4 and CFD underpredict more than 33% compared to measurement data, while CFD-VIT-RIT reduces the error to less than 15%. In Figure 2(b), since turbulence induced by the road surface thermal effects can be ignored in the winter, the differences in CALINE4 and CFD-VIT-RIT predictions are relatively small. However, CFD still shows big error due to no-consideration of VIT and RIT. The simulation results for I-710 in the summer and winter are shown in Figure 2(c) and Figure 2(d). The improvement of predictions by CFD-VIT-RIT over CFD and CALINE4 on I-710 can be attributed to the detailed treatment of VIT and RIT.

The horizontal dispersion of CO is determined mainly by wind velocity and turbulence (38). To compare near-road dispersions for both I-405 and I-710 in different seasons, we introduce a parameter called the dilution ratio, which is the

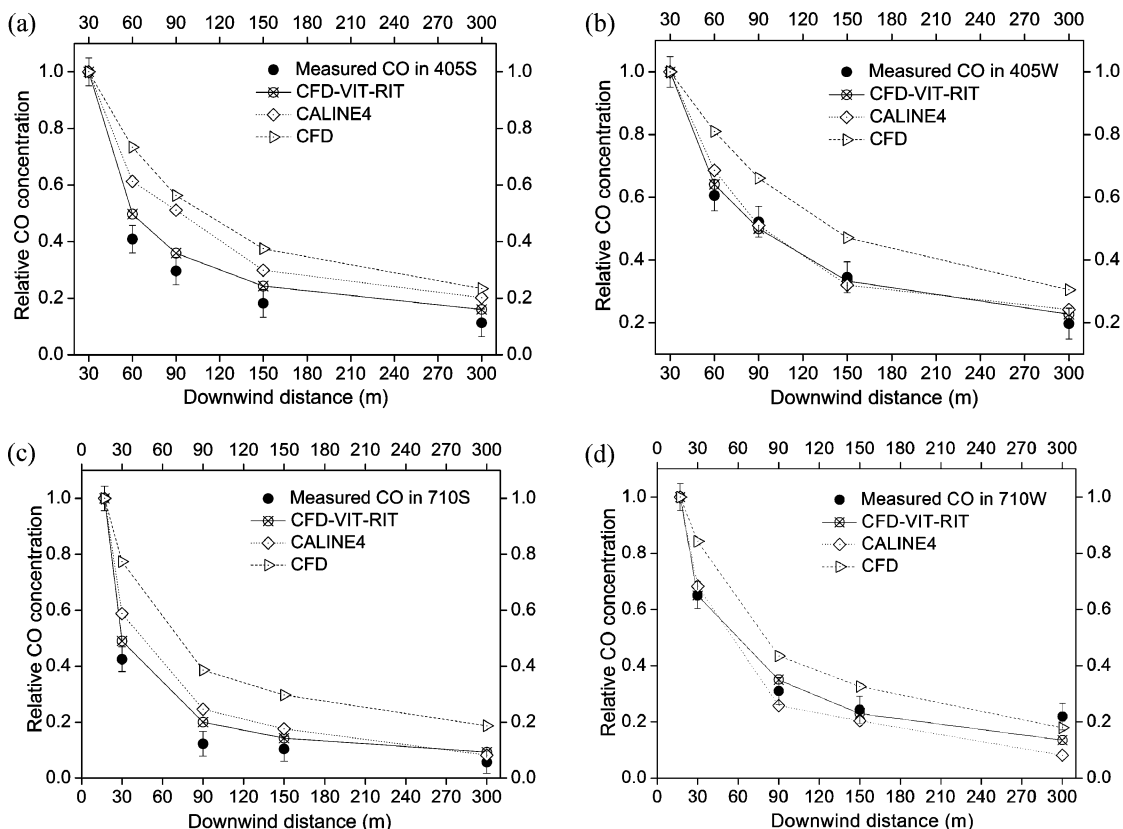


**FIGURE 2.** Comparison of relative CO concentrations between models and field experiment for I-405 in summer (a) and winter (b) and for I-710 in summer (c) and winter (d).

**TABLE 2.** RMS of Relative CO Concentration and Dilution Ratio between 30 and 150 m

		measurement	CFD-VIT-RIT	CALINE4	CFD
405S horizontal	30 m/150 m	5.5	4.11	3.34	2.67
	rms	N/A	0.065	0.186	0.270
405W horizontal	30 m/150 m	2.89	3.00	3.13	2.12
	rms	N/A	0.031	0.052	0.162
710S horizontal	30 m/150 m	4.12	3.43	3.32	2.61
	rms	N/A	0.064	0.124	0.277
710W horizontal	30 m/150 m	2.78	2.83	3.37	2.58
	rms	N/A	0.024	0.042	0.131
405S vertical	rms	N/A	0.059	0.246	0.213

ratio of background-subtracted CO concentrations at 30 and 150 m, listed in Table 2. The root-mean-square (rms) of measured and simulated relative CO concentrations at 60 m, 90 m, and 150 m for I-405 and 30 m, 90 m, and 150 m for I-710, respectively, is also shown in Table 2. More details can be found in ref 10. From Table 2, it is clear that due to the thermal effects, dilution ratios between 30 and 150 m in the summer are much larger than those of winter for both highways. Seasonal effects are significant with winters generally less dynamic than summers; therefore, thermal effects cannot be neglected during the summer, especially under low wind conditions and wind perpendicular to the street (10, 16, 29, 49). Mainly due to the existence of the embankment, dilution ratios of I-405 are higher than that of I-710 for both seasons with similar total TKE values. The dilution ratios obtained from CFD-VIT-RIT show the same trend as the measurement data, while CFD and CALINE4 show little change between different seasons. rms of CFD-VIT-RIT is consistently smaller than those of CALINE4 and CFD, which shows a more precise prediction of dilution ratio for CO horizontal dispersion and seasonal variations. CFD-VIT-RIT's capability in capturing the seasonal variations is

particular useful in long-term human exposure assessment of near-road exposure.

**Vertical Gradients.** We first compare the simulated wind velocity vertical profile with the field measurement. As illustrated in Figure S2 in the Supporting Information, the measured wind velocities are approximately constant with vertical height and have relatively small and similar standard deviations (38). CFD-VIT-RIT shows good consistence, except at height 0.6 m, where the simulated velocity is not within the standard deviation of the measured data. A possible reason is that since the sampling point is close to the surface, it is probably disturbed by the unconsidered structure on the ground.

Next, we compare the measured and simulated vertical profile of relative CO concentrations at eight sampling locations above the ground at 50 m downwind of I-405 horizontally in the summer, depicted in Figure 3(a). The vertical CO concentration is observed to reach a maximum at a height around 5 m above the ground and decreases by 30% at 18 m above the ground. There is a dimple observed at 10 m, which is likely due to secondary mixing above the central line of emission (38). CFD-VIT-RIT demonstrates great

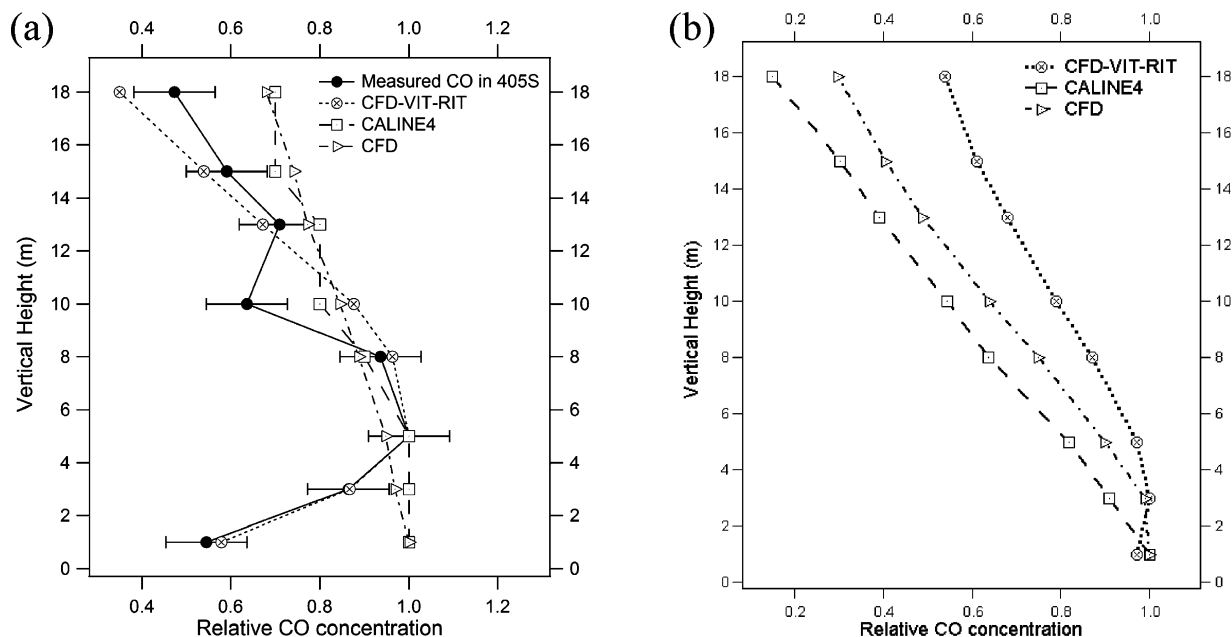


FIGURE 3. Comparison of vertical relative CO concentration for I-405 in the summer (a), and for I-710 in the summer (b).

superiority in predicting CO vertical profile compared to CALINE4 and CFD. The rms of CFD-VIT-RIT shown in Table 2 is nearly one-quarter of those of CALINE4 and CFD. VIT and RIT play more significant roles in the vertical dispersion, where turbulence dominates the mixing process, than in the horizontal dispersion, where both turbulence and axial wind transport govern the mixing process. CFD-VIT-RIT yields good predictions at almost all sampling points. Its maximum concentration is obtained at 6.4 m, about 1.9 m above the highway. The small rise of the plume from the highway is mainly due to the buoyancy of the exhaust induced by a higher temperature on surface of asphalted road. However, because of the strong mechanical mixing due to moving vehicles on road, the plume rise is small (14). Simulated CO concentration at the height of 0.6 m is in good agreement with the measurement data, though simulated wind velocity shows an error. This is mainly because vertical dispersion is mostly controlled by turbulence rather than wind velocity. The capability of CFD-VIT-RIT to accurately predict the vertical profiles of air pollutants is important in studying human exposure to near-road air pollution for people living at different elevations.

Figure 3(b) compares the simulated CO vertical profiles at 50 m from I-710 in the summer by CFD-VIT-RIT, CALINE4, and CFD models. CFD-VIT-RIT predicts maximum concentration around 2 m above the highway (at the ground level) due to the thermal effects. In contrast, the maximum concentrations predicted by CALINE4 and CFD are both at the ground level due to lack of representation of the thermal effects.

**On-Road Emission Factors of Carbon Monoxide.** As the capability of CFD-VIT-RIT has been validated by the horizontal and vertical gradients of CO, we apply the inverse modeling method to derive the on-road CO emission factors using CFD-VIT-RIT, following the methodology reported earlier (37). The derived CO emissions factors are, in  $\text{g mile}^{-1} \text{ vehicle}^{-1}$ , 6.1 for 405S, 7.2 for 405W, 7.0 for 710S, and 6.0 for 710W, which are similar to the values reported in the earlier study (37).

### Implications

We have demonstrated that the significant improvement in predicting the spatial gradients of air pollutants near roadways can be achieved by incorporating detailed treatment of VIT and RIT into dispersion modeling. RIT is

determined by the roadway design characteristics such as roadway configurations (e.g., elevated or depressed), road surface properties (e.g., asphalt or concrete), and roadside structures (e.g., noise and vegetation barriers). VIT is governed by the traffic mix on the roadways, which is, to a large extent, affected by roadway designs such as road width, slope and speed limits. Given the large effects of VIT and RIT on pollutant dispersion, we argue that roadway designs affect near-road air quality and that future roadway designs could serve as an effective strategy to mitigating near-road air pollution. Nevertheless, further understanding of the effects of the roadway designs on pollution dispersion is needed before making scientifically sound policies. We hope that our study can initiate future investigations into this subject.

CFD-VIT-RIT is still more computationally expensive than Gaussian plume models such as CALINE4, but it is able to provide much more physical insights thanks to its rigorous treatment of turbulence mixing mechanisms on- and near-road, evinced by the excellent prediction of vertical gradients of air pollutants near roadways. Thus CFD-VIT-RIT, or a combination of CFD-VIT-RIT and CALINE4, can become a valuable tool in roadway design process and near-roadway air quality research. The caveat is that a CFD model without detailed treatment of VIT and RIT adds no more benefits than CALINE4 besides high computational cost.

### Acknowledgments

The authors would like to acknowledge New York State Energy Research and Development Authority (NYSERDA) and University Transportation Research Center (UTRC) for the funding support.

### Supporting Information Available

Meteorological and road data, governing equations for  $k - \epsilon$  turbulence model, meshed vehicle model for I-710, and wall function for the fully developed vertical profile of inlet wind flow. This material is available free of charge via the Internet at <http://pubs.acs.org>.

### Literature Cited

- (1) Hagler, G. S. W.; Baldauf, R. W.; Thoma, E. D.; Long, T. R.; Snow, R. F.; Kinsey, J. S.; Oudejans, L.; Gullett, B. K. Ultrafine particles

- near a major roadway in Raleigh, North Carolina: Downwind attenuation and correlation with traffic-related pollutants. *Atmos. Environ.* **2009**, *43* (6), 1229–1234.
- (2) Westerdahl, D.; Wang, X.; Pan, X. C.; Zhang, K. M. Characterization of on-road vehicle emission factors and microenvironmental air quality in Beijing, China. *Atmos. Environ.* **2009**, *43* (3), 697–705.
- (3) Samet, J. M. Traffic, air pollution, and health. *Inhalation Toxicol.* **2007**, *19* (12), 1021–1027.
- (4) Peters, A.; von Klot, S.; Heier, M.; Trentinaglia, I.; Hormann, A.; Wichmann, H. E.; Lowel, H. Exposure to traffic and the onset of myocardial infarction. *New Engl. J. Med.* **2004**, *351* (17), 1721–1730.
- (5) McConnell, R.; Berhane, K.; Yao, L.; Jerrett, M.; Lurmann, F.; Gilliland, F.; Kunzli, N.; Gauderman, J.; Avol, E.; Thomas, D.; Peters, J. Traffic, susceptibility, and childhood asthma. *Environ. Health Perspect.* **2006**, *114* (5), 766–772.
- (6) Baldauf, R.; Thoma, E.; Khlystov, A.; Isakov, V.; Bowker, G.; Long, T.; Snow, R. Impacts of noise barriers on near-road air quality. *Atmos. Environ.* **2008**, *42* (32), 7502–7507.
- (7) Riddle, A.; Carruthers, D.; Sharpe, A.; McHugh, C.; Stocker, J. Comparisons between FLUENT and ADMS for atmospheric dispersion modelling. *Atmos. Environ.* **2004**, *38* (7), 1029–1038.
- (8) Zhang, K. M.; Wexler, A. S. Evolution of particle number distribution near roadways--Part I: analysis of aerosol dynamics and its implications for engine emission measurement. *Atmos. Environ.* **2004**, *38* (38), 6643–6653.
- (9) Fraigneau, Y. C.; Gonzalez, M.; Coppalle, A. Dispersion and chemical-reaction of a pollutant near a motorway. *Sci. Total Environ.* **1995**, *169* (1–3), 83–91.
- (10) Zhang, K. M.; Wexler, A. S.; Zhu, Y. F.; Hinds, W. C.; Sioutas, C. Evolution of particle number distribution near roadways. Part II: the 'road-to-ambient' process. *Atmos. Environ.* **2004**, *38* (38), 6655–6665.
- (11) Rao, S. T.; Sedefian, L. Characteristics of turbulence and dispersion of pollutants near major highways. *J. of Appl. Meteorol.* **1979**, *18* (3), 283–293.
- (12) Singh, N.; Joshi, R. R.; Chun, H. Y.; Pant, G. B.; Damle, S. H.; Vashishtha, R. D. Seasonal, annual and inter-annual features of turbulence parameters over the tropical station Pune (18 degrees 32 ' N, 73 degrees 51 ' E) observed with UHF wind profiler. *Ann. Geophys.* **2008**, *26* (12), 3677–3692.
- (13) Chock, D. P. General-Motors sulfate dispersion experiment - An analysis of the wind-field near a road. *Boundary-Layer Meteorol.* **1980**, *18* (4), 431–451.
- (14) Rao, K. S.; Gunter, R. L.; White, J. R.; Hosker, R. P. Turbulence and dispersion modeling near highways. *Atmos. Environ.* **2002**, *36* (27), 4337–4346.
- (15) Hauf, T.; Neumannhauf, G. The turbulent wind flow over an embankment. *Boundary-Layer Meteorol.* **1982**, *24* (3), 357–369.
- (16) Kim, J.-J.; Baik, J.-J. Urban street-canyon flows with bottom heating. *Atmos. Environ.* **2001**, *35* (20), 3395–3404.
- (17) Sini, J. F.; Anquetin, S.; Mestayer, P. G. Pollutant dispersion and thermal effects in urban street canyons. *Atmos. Environ.* **1996**, *30* (15), 2659–2677.
- (18) Xie, X. M.; Huang, Z.; Wang, J. S.; Xie, Z. The impact of solar radiation and street layout on pollutant dispersion in street canyon. *Build. Environ.* **2005**, *40* (2), 201–212.
- (19) Gromke, C.; Buccolieri, R.; Di Sabatino, S.; Ruck, B. Dispersion study in a street canyon with tree planting by means of wind tunnel and numerical investigations - Evaluation of CFD data with experimental data. *Atmos. Environ.* **2008**, *42* (37), 8640–8650.
- (20) Lidman, J. K. Effect of a noise wall on snow accumulation and air quality. *Transp. Res. Rec.* **1985**, *1033*, 79–88.
- (21) Benson, P. E. A Review of the Development and Application of the Caline3 and Caline4 Models. *Atmos. Environ. Part B-Urban Atmos.* **1992**, *26* (3), 379–390.
- (22) Cimorelli, A. J.; Perry, S. G.; Venkatram, A.; Weil, J. C.; Paine, R. J.; Wilson, R. B.; Lee, R. F.; Peters, W. D.; Brode, R. W. AERMOD: A Dispersion Model for Industrial Source Applications. Part I: General Model Formulation and Boundary Layer Characterization. *J. Appl. Meteorol.* **2005**, *44* (5), 682–693.
- (23) Cook, R.; Isakov, V.; Touma, J. S.; Benjey, W.; Thurman, J.; Kinnee, E.; Ensley, D. Resolving local-scale emissions for modeling air quality near roadways. *J. Air Waste Manage. Assoc.* **2008**, *58* (3), 451–461.
- (24) Venkatram, A.; Isakov, V.; Yuan, J.; Pankratz, D. Modeling dispersion at distances of meters from urban sources. *Atmos. Environ.* **2004**, *38* (28), 4633–4641.
- (25) Coe, D. L.; Eisinger, D. S.; Prouty, J. D.; Kear, T. *User's Guide for CLA: A User Friendly Interface for the CALINE4 Model for Transportation Project Impact Assessments*; Caltrans-U.C. Davis Air Quality Project, Sacramento, 1998.
- (26) Benson, P. E. A review of the development and application of the CALINE3 and CALINE4 models. *Atmos. Environ. Part B-Urban Atmos.* **1992**, *26* (3), 379–390.
- (27) Sahlodin, A. M.; Sotudeh-Gharebagh, R.; Zhu, Y. F. Modeling of dispersion near roadways based on the vehicle-induced turbulence concept. *Atmos. Environ.* **2007**, *41* (1), 92–102.
- (28) Katolicky, J.; Jicha, M. Eulerian-Lagrangian model for traffic dynamics and its impact on operational ventilation of road tunnels. *J. Wind Eng. Ind. Aerodynamics* **2005**, *93* (1), 61–77.
- (29) Xie, X.; Liu, C.-H.; Leung, D. Y. C. Impact of building facades and ground heating on wind flow and pollutant transport in street canyons. *Atmos. Environ.* **2007**, *41* (39), 9030–9049.
- (30) Liu, C. S.; Ahmadi, G. Computer simulation of pollutant transport and deposition near Peace Bridge. *Part. Sci. Technol.* **2005**, *23* (2), 109–127.
- (31) Ozdemir, E.; Ozdemir, I. B. Turbulent structure of three-dimensional flow behind a model car: 2. Exposed to crosswind. *J. Turbul.* **2004**, *5*, 18.
- (32) Kozaka, E. O.; Ozkan, G.; Ozdemir, I. B. Turbulent structure of three-dimensional flow behind a model car: 1. Exposed to uniform approach flow. *J. Turbul.* **2004**, *5*, 22.
- (33) Baumer, D.; Vogel, B.; Fiedler, F. A new parameterisation of motorway-induced turbulence and its application in a numerical model. *Atmos. Environ.* **2005**, *39* (31), 5750–5759.
- (34) Kalthoff, N.; Baumer, D.; Corsmeier, U.; Kohler, M.; Vogel, B. Vehicle-induced turbulence near a motorway. *Atmos. Environ.* **2005**, *39* (31), 5737–5749.
- (35) Garbrecht, T.; Lupkes, C.; Augstein, E.; Wamser, C. Influence of a sea ice ridge on low-level airflow. *J. Geophys. Res., [Atmos.]* **1999**, *104* (D20), 24499–24507.
- (36) Kim, H. G.; Patel, V. C. Test of turbulence models for wind flow over terrain with separation and recirculation. *Boundary-Layer Meteorol.* **2000**, *94* (1), 5–21.
- (37) Zhang, K. M.; Wexler, A. S.; Niemeier, D. A.; Zhu, Y. F.; Hinds, W. C.; Sioutas, C. Evolution of particle number distribution near roadways. Part III: Traffic analysis and on-road size resolved particulate emission factors. *Atmos. Environ.* **2005**, *39* (22), 4155–4166.
- (38) Zhu, Y. F.; Hinds, W. C. Predicting particle number concentrations near a highway based on vertical concentration profile. *Atmos. Environ.* **2005**, *39* (8), 1557–1566.
- (39) Zhu, Y. F.; Hinds, W. C.; Kim, S.; Shen, S.; Sioutas, C. Study of ultrafine particles near a major highway with heavy-duty diesel traffic. *Atmos. Environ.* **2002**, *36* (27), 4323–4335.
- (40) Zhu, Y. F.; Hinds, W. C.; Shen, S.; Sioutas, C. Seasonal trends of concentration and size distribution of ultrafine particles near major highways in Los Angeles. *Aerosol Sci. Technol.* **2004**, *38*, 5–13.
- (41) *Fluent 6.3.26 -User's Guide*; Fluent Inc.: 2006.
- (42) Thompson, R. S.; Eskridge, R. E. Turbulent diffusion behind vehicles: Experimentally determined influence of vortex pair in vehicle wake. *Atmos. Environ.* **1987**, *21* (10), 2091–2097.
- (43) Gidhagen, L.; Johansson, C.; Omstedt, G.; Langner, J.; Olivares, G. Model simulations of NOx and ultrafine particles close to a Swedish highway. *Environ. Sci. Technol.* **2004**, *38* (24), 6730–6740.
- (44) White, F. M. *Fluid Mechanics*; McGraw-Hill Science Engineering: 2002.
- (45) Terjung, W. H.; Orouke, P. A. The effects of changing solar angles, cloud regimes, and air temperatures on the temperatures of contrasting surfaces. *Boundary-Layer Meteorol.* **1982**, *24* (3), 269–279.
- (46) Khare, M.; Chaudhry, K. K.; Gowda, R. M. M.; Ahmad, K. Effects of the homogeneous traffic on vertical dispersion parameter in the near field of roadways - A wind tunnel study. *Environ. Model. Assess.* **2005**, *10* (1), 55–62.
- (47) Cook, R.; Touma, J. S.; Fernandez, A.; Brzezinski, D.; Bailey, C.; Scarbro, C.; Thurman, J.; Strum, M.; Ensley, D.; Baldauf, R. Impact of underestimating the effects of cold temperature on motor vehicle start emissions of air toxics in the United States. *J. Air Waste Manage. Assoc.* **2007**, *57* (12), 1469–1479.
- (48) Ban-Weiss, G. A.; McLaughlin, J. P.; Harley, R. A.; Lunden, M. M.; Kirchstetter, T. W.; Kean, A. J.; Strawa, A. W.; Stevenson, E. D.; Kendall, G. R. Long-term changes in emissions of nitrogen oxides and particulate matter from on-road gasoline and diesel vehicles. *Atmos. Environ.* **2008**, *42* (2), 220–232.
- (49) Xie, X. M.; Liu, C. H.; Leung, D. Y. C.; Leung, M. K. H. Characteristics of air exchange in a street canyon with ground heating. *Atmos. Environ.* **2006**, *40* (33), 6396–6409.